Fault Detection System for ICRF Transmission Line in LHD

K. Saito[a], T. Seki[a], H. Kasahara[a], R. Seki[a], S. Kamio[a], G. Nomura[a], T. Mutoh[b]

[a]*National Institute for Fusion Science, National Institutes of Natural Sciences, Toki, Gifu 509-5292, Japan*
[b]*Chubu University, Kasugai, Aichi 487-8501, Japan*

The transmission line is one of the most important components of ion cyclotron range of frequencies (ICRF) heating devices. In the case of unexpected trouble on the line, such as a breakdown, immediate power-off is necessary in order to avoid severe damage on the line. Breakdowns are difficult to detect with a reflection monitor, since the reflection may originate from a change in the antenna-plasma coupling. In the Large Helical Device (LHD), a Fault Detection System (FDS) for the transmission line was developed, which detects the breakdown utilizing the unbalance of three signals from the both ends of the line. For the precise balancing in the normal condition, the calibration is iteratively conducted. FDS is insensitive to the change of the antenna impedance, therefore, FDS can detect breakdown clearly. Frequency shift is also detectable with the FDS applied to a long transmission line. Therefore, the self-oscillation accompanying frequency shift could be detected in addition to breakdown.

Keywords: fault detection system, ICRF heating, LHD, transmission line, breakdown, self-oscillation

1. Introduction

Ion cyclotron range of frequencies (ICRF) heating is one of the plasma heating methods in the Large Helical Device (LHD) [1]. High-frequency power of approximately 1 MW can be fed from the final power amplifier (FPA) [2] to the ICRF antenna [3] via an impedance matching device [4] using a transmission line. Problems, such as melting caused by breakdown, have occurred on the line between the FPA and the impedance matching device in the LHD. In the case of trouble on the line, immediate power-off is necessary in order to avoid severe damage, such as melting, which can cause a fire, especially during long-pulse operation [5, 6]. The impedance matching device is located near the LHD, because the shorter the distance between the ICRF antenna and the matching device, the better for reducing power loss. As a result, the distance between the FPA and the impedance matching device reaches more than 100 m. Moreover, the route of the line is complicated. Therefore, it is difficult to monitor the temperature all the way along the line in order to detect the breakdown. It is also difficult to recognize faults by reflected power, since the increase in reflection may be caused by the normal variation of the antenna-plasma coupling. For these reasons, we developed a Fault Detection System (FDS) for the ICRF transmission line in the LHD by applying the technique of the Scattering Matrix Arc Detection (SMAD) system in the JET ITER-like ICRF antenna [7], which is sensitive only to the change in the S-matrix of the antenna caused by arcing, and is insensitive to the antenna-plasma coupling.

The principles and setup of the FDS are described in section 2. In section 3, we introduce a newly developed calibration method. Simulation of FDS is presented in section 4. Section 5 presents the results of a low-power test, and section 6 is the conclusion.

2. Principle and setup of FDS

We assume that ports 1 and 2 are the input and output ports, respectively, of a transmission line. V_{f1} and V_{r1} are the forward and the reflected wave voltages at port 1, and V_{f2} and V_{r2} are the forward and the reflected wave voltages at port 2. The relation between these voltages can be written with the S-matrix as

$$\begin{pmatrix} V_{r1} \\ V_{f2} \end{pmatrix} = \begin{pmatrix} S_{11} & S_{12} \\ S_{21} & S_{22} \end{pmatrix} \begin{pmatrix} V_{f1} \\ V_{r2} \end{pmatrix}. \quad (1)$$

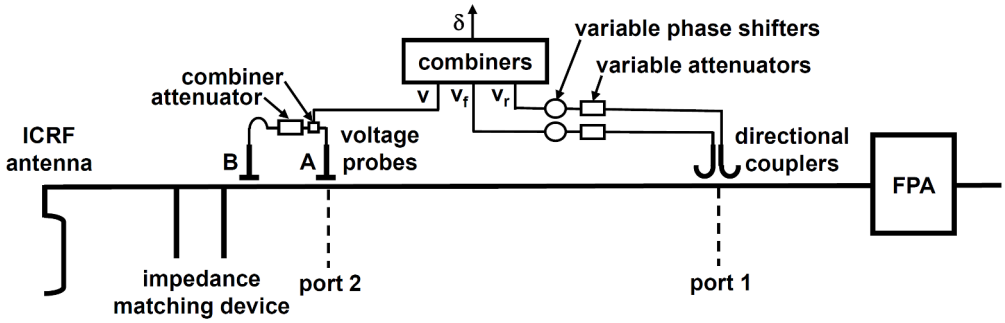

Fig. 1 Configuration of detectors on the transmission line and outer circuit for FDS.

author's email: saito@nifs.ac.jp

V_2 is the combined voltage of V_{f2} and V_{r2} defined as

$$V_2 \equiv c_f V_{f2} + c_r V_{r2} . \quad (2)$$

By eliminating V_{f2} and V_{r2} from Eqs. (1) and (2), the following relation is derived:

$$V_2 - \{c_f (S_{21} - \frac{S_{11}S_{22}}{S_{12}}) - c_r \frac{S_{11}}{S_{12}}\} V_{f1} - (c_f \frac{S_{22}}{S_{12}} + \frac{c_r}{S_{12}}) V_{r1} = 0 . \quad (3)$$

The left-hand side is independent of output impedance. Therefore, if the left-hand side deviates from zero, this means that the S-matrix has changed, and there is a fault in the line.

The FDS simulates Eq. (3) in the outer circuit, as shown in Fig. 1. Assuming that v is the voltage of the detected signal for V_2 with the coupling factor c_2 (=v/V_2), Eq. (3) is written with the definition of δ as

$$\delta \equiv v + v_f + v_r = 0 \quad (4)$$

where v_f and v_r are defined as follows:

$$\begin{cases} v_f = -c_2 \{c_f (S_{21} - \frac{S_{11}S_{22}}{S_{12}}) - c_r \frac{S_{11}}{S_{12}}\} V_{f1} \\ v_r = -c_2 (c_f \frac{S_{22}}{S_{12}} + \frac{c_r}{S_{12}}) V_{r1} . \end{cases} \quad (5)$$

The two values v_f and v_r can be generated by adjusting the forward and the reflection signals from the existing directional couplers at the outlet of the FPA, which is used for the impedance matching and the power monitoring. The adjustment is conducted with variable attenuators and phase shifters inserted in the lines of the forward and reflection signals. In order to avoid the nonlinearity caused by the variable attenuators and phase shifters, input signals must be sufficiently attenuated. Although v is generated with a combination of forward and reflected wave voltages at port 2, v can be easily generated with a combination of voltages at separate positions, as shown in Fig. 1. We used the combined voltage signal from two voltage probes for v, since there are voltage probe ports near the inlet of the impedance matching device. The summation of v, v_f, and v_r was realized with power combiners to generate the combined signal δ. This signal was then amplified, and bandpass filters were inserted to cut RF noise from the plasma. The signal was converted to a DC signal and connected to a comparator and an analog-digital converter through a low-pass filter. Due to the long distance between the directional couplers and the voltage probes, there is a time lag between signals. The low-pass filter was thus needed to ignore the finite δ at the timing of instantaneous turning on or off induced by the time lag. If the three signals lose balance in spite of the proper adjustment of phase shifters and attenuators, the finite combined signal δ is generated. This indicates that there is a fault somewhere in the transmission line, because the S-matrix has been changed, and the FDS will turn off the power before amplification. For a large |δ|, the comparator outputs an off-signal instantaneously. However, the combined signal δ depends on the power. Therefore, the normalized combined signal defined as follows is used for the sensitive judgment of faults:

$$\delta_n = \frac{\delta}{\sqrt{|v|^2 + |v_f|^2 + |v_r|^2}} . \quad (6)$$

Self-oscillations sometimes occur in the FPA without input power, which may cause damage on ICRF devices. This accompanies the frequency shift that changes the S-matrix of the transmission line. Therefore, the FDS can also detect self-oscillation. If the power was turned off by the FDS before amplification however, the FDS still detected faults, then in such a case bias voltages on the anode and screen grid in the FPA will be dropped because the FDS identified it as a self-oscillation.

3. Iterative calibration

Normally, output impedance of the transmission line is adjusted to the characteristic impedance of the line of 50 Ω with the impedance matching device. However, the output impedance sometimes differs from the characteristic impedance due to the fast variation of antenna impedance. Therefore, the balance of the three signals must be maintained with arbitrary output impedance. Adjustment of phase shifters and attenuators based on Eq. (5) is possible in principle. However, all parameters in Eq. (5) and coupling factors of forward and reflected waves at the directional couplers must be measured or simulated as the SMAD in JET. Moreover, the dependences of attenuation and phase shift on control voltages must be determined. There will be a limitation in terms of accuracy with this method. For sensitive fault detection, therefore, we developed an iterative calibration method. In this method, adjustments of phase shifters and attenuators were conducted with the following procedure. First, v_f, v_r, and δ are measured using an oscilloscope, and v is deduced from Eq. (4):

$$v_{1,2} = \delta_{1,2} - v_{f1,2} - v_{r1,2} \quad (7)$$

where the output impedance is changed twice with the impedance matching device, as indicated by the suffixes 1 and 2. Assuming that forward and reflection signals are adjusted in order to reduce the combined voltage δ in arbitrary output impedance with phase shifters and attenuators as

$$v_f' = \alpha v_f \text{ and } v_r' = \beta v_r , \quad (8)$$

the expected voltages of combined signals are written as follows:

$$\begin{cases} \delta_1' = v_1 + v_{f1}' + v_{r1}' = v_1 + \alpha v_{f1} + \beta v_{r1} \\ \delta_2' = v_2 + v_{f2}' + v_{r2}' = v_2 + \alpha v_{f2} + \beta v_{r2} . \end{cases} \quad (9)$$

These combined signals $\delta_{1,2}'$ should be zero. Therefore, the following equation is derived using Eq. (7),

$$\begin{cases} \alpha v_{f1} + \beta v_{r1} = -\delta_1 + v_{f1} + v_{r1} \\ \alpha v_{f2} + \beta v_{r2} = -\delta_2 + v_{f2} + v_{r2} . \end{cases} \quad (10)$$

Therefore, adjustment factors α and β are determined:

$$\begin{cases} \alpha = (-v_{r2}\delta_1 + v_{r1}\delta_2)/(v_{f1}v_{r2} - v_{r1}v_{f2}) + 1 \\ \beta = (v_{f2}\delta_1 - v_{f1}\delta_2)/(v_{f1}v_{r2} - v_{r1}v_{f2}) + 1. \end{cases} \quad (11)$$

Phase shifters and attenuators are adjusted according to the determined α and β. Adjustment factors α and β are determined so that the combined signals $\delta_{1,2}$ are zero. Therefore, $\delta_{1,2}$ will be smaller than $\delta_{1,2}$ before the adjustment. As a result, $\delta_{1,2}$ will converge to zero in arbitrary output impedance by repeating this procedure several times.

4. FDS simulation

In order to investigate the behavior of the FDS, a simulation was conducted at the frequency of 38.47 MHz used in ICRF heating experiments in the LHD assuming the ideal transmission line ($S_{11}=S_{22}=0$ and $S_{12}=S_{21}=e^{-jkL}$, where k is the wave number in the transmission line and L is the line length).

4.1 Single- and double-probe methods

In this simulation, the breakdown resistances R_b=10, 100, and 1000 Ω were inserted between the inner and outer conductors of the transmission line with the output impedance of 50 Ω. The single-probe method was simulated first, which is simple and similar to the SMAD in JET. The voltage probe was located at x=0. In the case of single probe method, c_f/c_r was 1, since the voltage in the transmission line is the sum of the forward and reflected wave voltages. Simulated results are plotted in Fig. 2(a). There were insensitive regions in the breakdown position around x=nλ/2, where n is an integer. The double-probe method was then simulated by locating two voltage probes at x=0 (probe A) and x=-λ/4=-1.95 m (probe B), respectively. The intensity of signal B was attenuated by -4.44 dB, and the phase of signal B was shifted by -90.0°. Then, the two signals were combined to generate signal v. In this case, c_f/c_r was ¼, and the insensitive regions disappeared in the FPA side of the voltage probe A, as shown in Fig. 2(b).

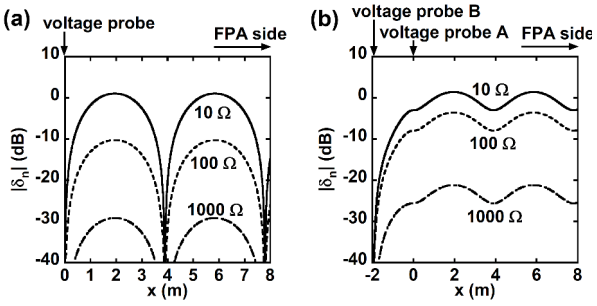

Fig. 2 The relation between breakdown position and the intensity of normalized combined signal $|\delta_n|$ with three different breakdown resistances for (a) the single-probe method and (b) the double-probe method.

4.2 The effect of expansion of transmission line

With long-pulse operation, the temperature of the entire transmission line may increase several degrees. In the case of a temperature rise of 10 °C and a line length of 150 m, expansion ΔL will be approximately 3.5 cm. The expansion ΔL changes the S-matrix and $|\delta_n|$ increases in the case of no reflection as follows:

$$|\delta_n| = \frac{|1 - e^{jk\Delta L}|}{\sqrt{2}}. \quad (12)$$

When ΔL increases up to 3.5 cm, $|\delta_n|$ reaches -34 dB. Therefore, the FDS functions to adjust the attenuators and phase shifters according to the temperature at a point on the transmission line for the sensitive detection of faults.

5. Test results

The test was conducted with the low power of less than 10 mW. Therefore, three signals were increased by amplifiers. The double-probe method was used to eliminate insensitive regions with the following parameters:

- Distance between voltage probes A and B: 6.09 m.
- Combination of signals: $v \propto V_A + 0.57e^{1.72j}V_B$
  $\propto V_{fA} + 3.6e^{0.06j}V_{rA}$

where V_A and V_B are the voltages in the transmission line at the positions of probe A and B, respectively. V_{fA} and V_{rA} are the forward and reflected wave voltages at the position of probe A, respectively.

5.1 Calibration

The impedance matching device changed the reflection ratio Γ, as shown in Fig. 3(a), where Γ is defined at the inlet of the matching device. The calibration was conducted at points C and E in Fig. 3(a). As shown in Fig. 3(b), calibration was repeated four times in order to reduce the intensity of combined signal δ, and finally $|\delta_n|$ reached nearly zero (<-35 dB≈noise level in this low power test) in the wide range of Γ. This means that the FDS is insensitive to the change of output impedance caused by the variation of antenna-plasma coupling.

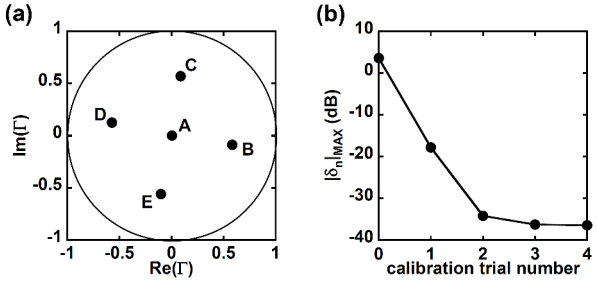

Fig. 3 (a) Five different complex reflection ratios realized by using the impedance matching device. Calibration was conducted with points C and E. (b) Reduction of $|\delta_n|_{MAX}$ by the iterative calibration, where $|\delta_n|_{MAX}$ means the maximum $|\delta_n|$ at the five points from A to E.

5.2 Breakdown simulation

Breakdown was simulated experimentally using the contactor shown in Fig. 4, although the real breakdown impedance is unknown. The distance between the voltage probe A and the contactor in the FPA side was 1.45 m. The impedance matching device was adjusted so that the reflection ratio decreased to zero. Various resistances were then attached to the port of the contactor one by one. The reflection ratio is written with the resistance R_b:

$$|\Gamma| = \left| \frac{Z_c}{Z_c + 2Z_b} \right| = \left| \frac{50\Omega}{50\Omega + 2(R_b + j\omega L_c)} \right| \quad (13)$$

where Z_c is the characteristic impedance of the line and Z_b is the breakdown impedance. The inductance of the contactor L_c was deduced from $|\Gamma|=0.59$ at $R_b=0$ as $L_c=1.42\times10^{-7}$ H. In the LHD, the interlock level of the reflected power ratio is 0.2; then $|\Gamma|$ is 0.45. Therefore, as shown in Fig. 5, when R_b is more than 20 Ω, the reflection interlock system does not function. On the other hand, fault signal $|\delta_n|$ was clearly increased from less than -35 dB to -20 dB even when the breakdown resistance was 1000 Ω ($|\Gamma|=0.037$), as shown in the figure.

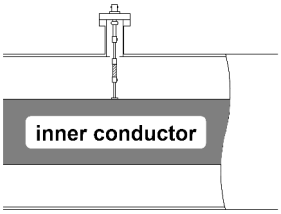

Fig. 4 The contactor for the simulation of breakdown.

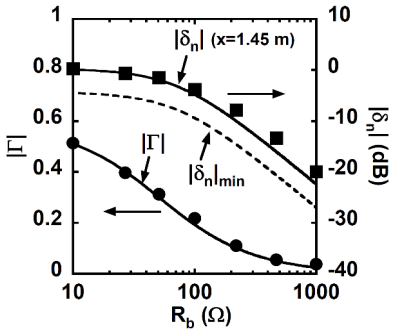

Fig. 5 Reflection ratio $|\Gamma|$ and the intensity of normalized combined signal $|\delta_n|$ with various resistances R_b. Plots are test results and solid lines are simulated results. Dashed line is the simulated minimum $|\delta_n|$ with scanning of the position of the contactor between the voltage probe A and the directional couplers.

5.3 Frequency-scan test for the simulation of self-oscillation

Figure 6(a) shows an example of the power spectrum of the self-oscillation signal during plasma experiments. The frequency of self-oscillation shifts by several hundred kHz from the original frequency of 38.47 MHz. The frequency shift is small, however, the S-matrix of the transmission line largely changes due to the long length of the line. A frequency-scan test was conducted to simulate self-oscillation. As shown in Fig. 6(b), $|\delta_n|$ clearly increased by the shift of frequency. This means that self-oscillation is detectable, and will be stopped by the dropping of bias voltages on anode and screen grid in the FPA.

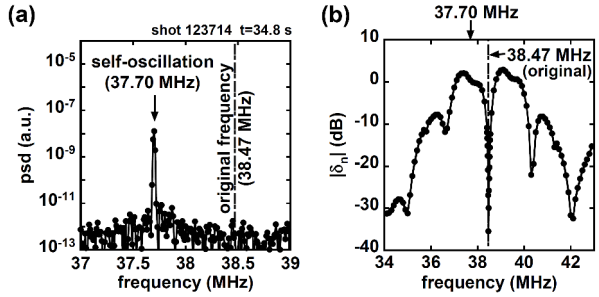

Fig. 6 (a) Power spectrum of self-oscillation signal detected by a magnetic probe installed in the LHD. (b) Increase in $|\delta_n|$ with the shift of frequency.

6. Conclusion

An FDS for the ICRF transmission line was developed for the safe ICRF operation in the LHD. This system is insensitive to the variation of antenna impedance, but is sensitive to the change of the S-matrix of the transmission line caused by some faults, which is the same as the SMAD in JET ITER-like ICRF antenna. The SMAD is for a short antenna. However, when this technique was applied to the line longer than one half-wave length, a problem of insensitive regions emerged. FDS simulation clarified that double-probe method would solve this problem. In the normal condition, a small fault signal is better. Otherwise, the threshold for the detection of a fault will be large, which will prevent the detection of minor faults. The iterative calibration method demonstrated that the fault signal decreases sufficiently in arbitrary output impedance. As a result, the normalized combined signal increased clearly with the breakdown simulation test, even when the reflection ratio was much smaller than the interlock level. Self-oscillation is also detectable with the FDS, since the small frequency shift caused by self-oscillation largely changes the S-matrix of the long transmission line. This fault detection system will be operated in the next ICRF heating experiments in the LHD following the high power calibration and the determination of the proper threshold for the detection of a fault signal.

Acknowledgements

The authors would like to thank the technical staff of the LHD Experiment Group at the National Institute for Fusion Science for their helpful support during this research. This work was supported by NIFS budget ULRR703.

References

[1] O. Kaneko, H. Yamada, S. Inagaki, M. Jakubowski, S. Kajita, S. Kitajima, et al., Nucl. Fusion 53 (2013) 104015.

[2] T. Seki, R. Kumazawa, T. Mutoh, F. Shimpo, G. Nomura, T. Watari, et al., Fusion Science and Technology 40 (2001) 253-264.

[3] K. Saito, T. Seki, H. Kasahara, R. Seki, S. Kamio, G. Nomura, T. Mutoh, Fusion Eng. Des. 96-97 (2015) 583-588.

[4] K. Saito, C. Takahashi, M. Yokota, G. Nomura, F. Shimpo, T. Seki, et al., Fusion Eng. Des. 83 (2008) 245-248.

[5] K. Saito, T. Mutoh, R. Kumazawa, T. Seki, Y. Nakamura, N. Ashikawa, et al., J. Nucl. Mater. 363-365 (2007) 1323-1328.

[6] S. Kamio, H. Kasahara, T. Seki, K. Saito, R. Seki, G. Nomura, et al., Fusion Eng. Des. 101 (2015) 226-230.

[7] M. Vrancken, E. Lerche, T. Blackman, F. Durodié, M. Evrard, M. Graham, et al., Fusion Eng. Des. 86 (2011) 522-529.